ACCEPTED VERSION

Linh Viet Nguyen, Kelly Hill, Stephen Warren-Smith, Tanya Monro
Interferometric-type optical biosensor based on exposed core microstructured optical fiber
Sensors and Actuators, B: Chemical, 2015; 221:320-327

Final publication at http://dx.doi.org/10.1016/j.snb.2015.06.068

Interferometric-type optical biosensor based on exposed core microstructured optical fiber

Linh Viet Nguyen [1,2,], Kelly Hill [1,3], Stephen Warren-Smith [2,4], and Tanya Monro [2,5,6]*

[1]Plant Biosecurity Cooperative Research Centre, Bruce, ACT 2617, Australia

[2] Institute for Photonics and Advanced Sensing and School of Physical Sciences, The University of Adelaide, Adelaide, SA 5005, Australia

[3] South Australian Research and Development Institute, 2b Hartley Grove, Urrbrae, SA 5064, Australia

[4] Currently with Leibniz Institute of Photonic Technology (IPHT), Albert-Einstein-Straße 9, 07745 Jena, Germany

[5] University of South Australia, Adelaide, SA 5000, Australia

[6] ARC Centre of Excellence for Nanoscale Biophotonics, The University of Adelaide, Adelaide, SA 5005, Australia

**linhnguyen.research@gmail.com*

Abstract: This work presents a novel biosensor using the multimode interference effect in an exposed core microstructured optical fiber (ECF). In this work biotin molecules are immobilized onto the ECF core surface to serve as the capturing probe for streptavidin, the target molecules. Since each distinct guided mode in the ECF interacts with the surrounding medium differently, the interference between any two specific modes will experience a fringe shift (or phase change) upon a change in the refractive index (RI) of the surrounding medium, or a localized RI change on the surface of the ECF core as a result of a biological binding event. In our experiment, the interferometric sensing platform was realized by splicing a section of ECF with lead-in and lead-out single mode fibers (SMFs). An interference pattern is obtained in the transmission spectrum as the result of multiple excited modes (excited and re-collected at the lead-in and lead-out splicing points) propagating in the ECF with different propagation constants. The interference pattern is non-uniform, indicating that there are more than two modes involved. Fast Fourier transform (FFT) is used to separate individual interference patterns that contribute to this complex spectrum and monitor their phase changes upon RI variation of the surrounding medium. In this way multiple RI sensitivities can be realized because each spatial frequency possesses a distinct sensitivity with respect to the surrounding RI. The operation of this device was validated by measuring the phase changes that occur when the sensing platform was subjected to solutions of different RIs or functionalized with different molecules. A biosensor was demonstrated based on this novel platform using biotin as the capturing probe to detect streptavidin with low non-specific adsorption. The proposed platform is reliable, cost-effective, and offers a potential label-free biosensing alternative to the widely used surface plasmon resonance (SPR) technique.

1. Introduction

Cost-effective and stable biosensing platforms are sought after for a wide range of applications such as medicine, agriculture, environmental monitoring, food control, safety, and security monitoring. There have been numerous reviews describing current and potential applications of biosensing devices and the preferred features of such a device [1-6]. Pathogen detection and identification is one such application [7]. This area is important in surveillance and health monitoring and also for diagnostics to facilitate appropriate treatment choices. The motivation for this work is the application of biosensors for pathogen monitoring in agriculture systems. For biosensors to aid in the progression of plant pathology and the increased efficiency of surveillance and/or diagnostic protocols in agriculture, a portable system capable of remote sensing is desired. In-field devices amenable to easy manual use for minimally trained users, or compatible with an autonomous detection system, require an all-in-one sensor-transducer-

display arrangement that is not reliant on excessive sample preparation or separation steps. Ideally the biosensor would detect the target (or targets if multiplexed detection is enabled) in an unprocessed sample with high specificity and sensitivity. To minimize sample preparation steps, as well as avoid problems associated with quantum yield losses and costs involved in colorimetric and fluorescent tags, a label free sensor platform would be advantageous. Label-free optical biosensors based on various optical effects such as surface plasmon resonance, optical cavities, interferometry, and fiber gratings have been widely investigated to date [8].

Optical interferometry is a well-established technique for analyzing changes in optical thickness or refractive index, and thus is a well-justified option for use in label-free biosensing. Whilst the majority of optical interferometric biosensors have been implemented with optical waveguides [9-11], optical fiber based implementation can offer an important addition as the fibers can be fusion-spliced together, leading to an all-fiber configuration. This eliminates the mechanically-induced errors often associated with optical alignment in bulk-optic systems and thus is particularly attractive for applications requiring portability such as in-field surveillance of pathogens. Optical fibers also offer a great potential for increased sensitivity through long interaction lengths, provided optical losses can be managed [12]. However, to facilitate interaction of the light propagating in the fiber core with the analyte for use in biosensing, chemical etching [13] or tapering [14] typically has to be carried out on the fibers, leading to inferior mechanical properties. More advanced designs of optical fibers such as photonic crystal fiber [15] or suspended core microstructured fiber [12, 16] can allow direct interaction of the light in the fiber core with the analyte solution flowing through the air-holes running along the fiber core. However, it is difficult to realize an all-fiber configuration in such cases because the air-holes need to be open to allow the flow of the solution through these holes.

To solve this issue we have developed a special type of optical fiber called exposed-core microstructured optical fiber (ECF) [17-19]. Of its many advantageous characteristics compared with conventional microstructured optical fibers, the most distinctive one is that ECF can be spliced with standard SMFs to form all-fiber configuration [20], while the light propagating in the core still has direct contact with analyte suspended in the surrounding medium thanks to the exposed core. Here we propose and experimentally demonstrate a novel platform for label-free biosensing that utilizes the multimode interference effect in an ECF. We use Fourier analysis to separate the individual interference patterns from the raw complex pattern obtained due to the fact that more than two modes are excited in the ECF, enabling the proposed platform to exhibit multiple and selectable sensitivities with respect to the surrounding refractive index (RI). Due to their very well known strong binding affinity [21], biotin and streptavidin are chosen as the receptor and target molecules to demonstrate the biosensing capability of the platform. The proposed platform is not restricted to just biotin-streptavidin, other types of receptor-target pairs such as cells, cell-surface proteins, enzymes, antibodies, and oligonucleotides could also be used on the proposed platform for developing biosensors for different purposes.

2. Methods

2.1. Multimode interference in exposed core microstructured optical fiber and the sensor's operational principle

ECF is a special type of microstructured optical fiber whose suspended core is exposed to the surrounding medium thanks to an open side of the ECF cladding [18]. It is typically fabricated by drilling holes along a silica rod [19] to form a suspended core fiber preform. One air hole of the preform is then cut or polished open, exposing the core to the surrounding medium on that side. The preform is then drawn with well-controlled pressure inside the holes into an ECF [20]. In this way, even if the ECF is spliced at both ends, liquid containing analyte can still have direct access to the evanescent field of light propagating along the core. Due to the high numerical aperture of ECF (glass-air or glass-water interfaces) and the difficulty in fabricating the ECF core small enough to support a single mode regime guidance (which requires sub-micrometer core diameters), the ECFs that have been developed to date are multimode fibers.

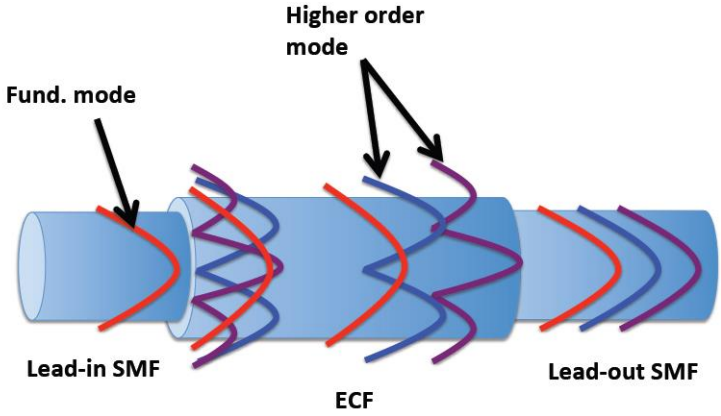

Fig. 1. Schematic diagram of the multimode interference that occurs in multimode ECFs. The fundamental mode of the lead-in SMF excites three different modes in the ECF which, after propagating through the ECF, converts again into the fundamental mode of the lead-out SMF but with a certain phase delay between each other. These phase delays result in an interference pattern in the transmission spectrum.

To estimate the number of modes that are supported by the ECF we have performed a simple calculation using a step-index optical fiber model, which we have used previously as an approximation for suspended-core microstructured optical fiber [22]. Using the refractive index values for silica glass as the core, air as the cladding, and a core diameter of 7.5 μm, a step-index fiber can propagate 68 modes. However, only a small subset of these is likely to be involved in the interferometer, depending on the coupling conditions into and out of the ECF.

Each mode propagates in the ECF core with a slightly different group velocity. The principle of operation can therefore be explained by referring to the schematic diagram of the SMF-ECF-SMF configuration in Fig. 1. At the splicing point between the lead-in SMF to the ECF, light from the fundamental mode of the lead-in SMF will be decomposed into different propagation modes of the ECF. After propagating through the ECF, those modes will recouple into the fundamental mode of the lead-out SMF experiencing a phase delay between each other due to different propagation constants. Thus an interference pattern can be formed in the transmission spectrum of the structure. Assuming negligible dispersion over a narrow wavelength bandwidth, the power after propagating the SMF-ECF-SMF structure can be described as:

$$I = \left\{ \sum_{i=1}^{n} \sqrt{I_i} e^{i b_i L_{ECF}} \right\}^2 = \sum_{i=1}^{n} I_i + \sum_{i \neq j=1}^{n} \sqrt{I_i I_j} \cos\left[\frac{2\pi}{\lambda} (n_i^{eff} - n_j^{eff}) L_{ECF} \right] \qquad (1)$$

where I_i and n_i^{eff} are the power portion carried in the corresponding *ith* mode of the ECF and its effective index, respectively. L_{ECF} is the ECF length and λ is the wavelength. It can be seen from Eq. 1 that in the general case the resultant interference pattern is a complex spectrum in the wavelength domain as it is the superposition of many individual interferences formed by a specific pair of excited modes {i,j} in the ECF. Since n_i^{eff} is highly sensitive with changes the ECF's cladding index which, in our particular case, is the ambient refractive index on the exposed core side as well as localized RI change on the ECF's core surface due to a biological binding event, a phase change or interference fringe shift will be induced and consequently such RI changes can be detected. For simplicity, assuming that only two modes of the ECF are dominantly excited, from Eq. 1 we have the simple two-beam (in this case, two-mode) interference equation:

$$I = I_1 + I_2 + 2\sqrt{I_1 I_2} \cos\left[\frac{2\pi}{\lambda} (n_1^{eff} - n_2^{eff}) L_{ECF} \right] \qquad (2)$$

Given a fixed ECF length L_{ECF} as well as mode effective indices n_1^{eff} and n_2^{eff} it can be seen from Eq. 2 that the total transmitted power is an interference pattern in the wavelength domain. Since in such domain the interference pattern is a simple periodical waveform, it corresponds to a

frequency in the spatial frequency domain obtained by applying a fast Fourier transform (FFT) to the wavelength spectrum. The phase term at this spatial frequency is given by the term:

$$f = \frac{2p}{l}(n_1^{eff} - n_2^{eff})L_{ECF} \quad (3)$$

With a change in the ambient RI, the effective indices of the modes will be modified and thus the phase term changes by the amount:

$$df = \frac{2p}{l}(dn_1^{eff} - dn_2^{eff})L_{ECF} = \frac{2p}{l}dn^{eff}L_{ECF} \quad (4)$$

It can be seen that $\delta\Phi$ will vary with respect to the change in the RI of the surrounding medium and the RI phase-sensitivity is dependent on δn^{eff} or how differently the two involved modes "see" the change in the surrounding RI. In addition the RI sensitivity of $\delta\Phi$ is linearly proportional to the ECF length, the longer the ECF length the more phase-sensitive. In the wavelength domain, the phase change will induce a wavelength shift of the interference fringe from the reference wavelength λ_0 as:

$$D\lambda = \frac{\lambda_0^2}{2p\Delta n^{eff}L_{ECF}}df = \frac{FSR}{2p}df \quad (5)$$

$$FSR = \frac{\lambda_0^2}{\Delta n^{eff}L_{ECF}} \quad (6)$$

where *FSR* is the free spectral range or the wavelength spacing between two adjacent minimas/maximas of the interference. Whilst the analysis in Eqs. 2-6 is for the simplified case of two mode interference, such individual interference patterns can always be obtained by applying an FFT on the complex wavelength spectrum of the multi-beam (multi-mode) interference. Then either the phase can be monitored at a specific spatial frequency or the filtered FFT peak can be converted back to the wavelength domain and the wavelength shift monitored in order to track the refractive index changes either in the bulk solution or due to a binding event on the ECF core surface.

2.2. Experimental procedure and measurement

A schematic diagram of the measurement setup for measuring streptavidin suspended in a buffer solution is shown in Fig. 2a. First, approximately 20 cm of an ECF (cross section of the ECF shown in the Fig. 2a inset) was spliced with two standard SMFs. The mode coupling was controlled by means of aligning the ECF and the SMF for maximum transmitted power through the ECF core using the in-built translation stages of a Fujikura fusion splicer (FSM-100P). We also optimized the splicing conditions for our particular case of standard SMFs (Corning SMF-28) [20] to achieve consistent coupling conditions. It should be noted that for a different type of SMF (e.g. small core, high-index contrast, depressed inner cladding etc) as well as ECFs with different parameters (e.g. core diameter, air-hole diameter, shape of strut etc), different optimized splicing conditions will be required. One port of a standard Fiber Bragg grating (FBG) interrogator (National Instruments PXIe 4844) was used as the light source (tunable laser) and another port was used as a photodetector to measure the transmission spectrum of the device. While the FBG interrogator is nominally designed for reflection mode operation, reflections in the setup were minimized using angled connectors and splices such that only transmission was recorded. The FBG interrogator has a spectral resolution of 4 pm. The ECF was enclosed in an in-house made flow cell (image shown in Fig. 2b) whose filling volume is approximately 0.8 ml with inlet and outlet ports for continuously filling and draining the flow cell. The FBG interrogator was computer-interfaced using a Labview program that captured the raw spectrum in the wavelength domain, applied an FFT, and monitored the phase change at a chosen spatial frequency for the entire duration of the experiment. Alternatively, an FFT filter can be applied on a chosen frequency, converted back to the wavelength spectrum and wavelength shifts monitored with respect to the functionalization

steps. We chose the frequency of highest intensity in the spatial frequency domain as it corresponds to the interference between the two most dominantly excited modes in the ECF for monitoring of the functionalization stages and detection.

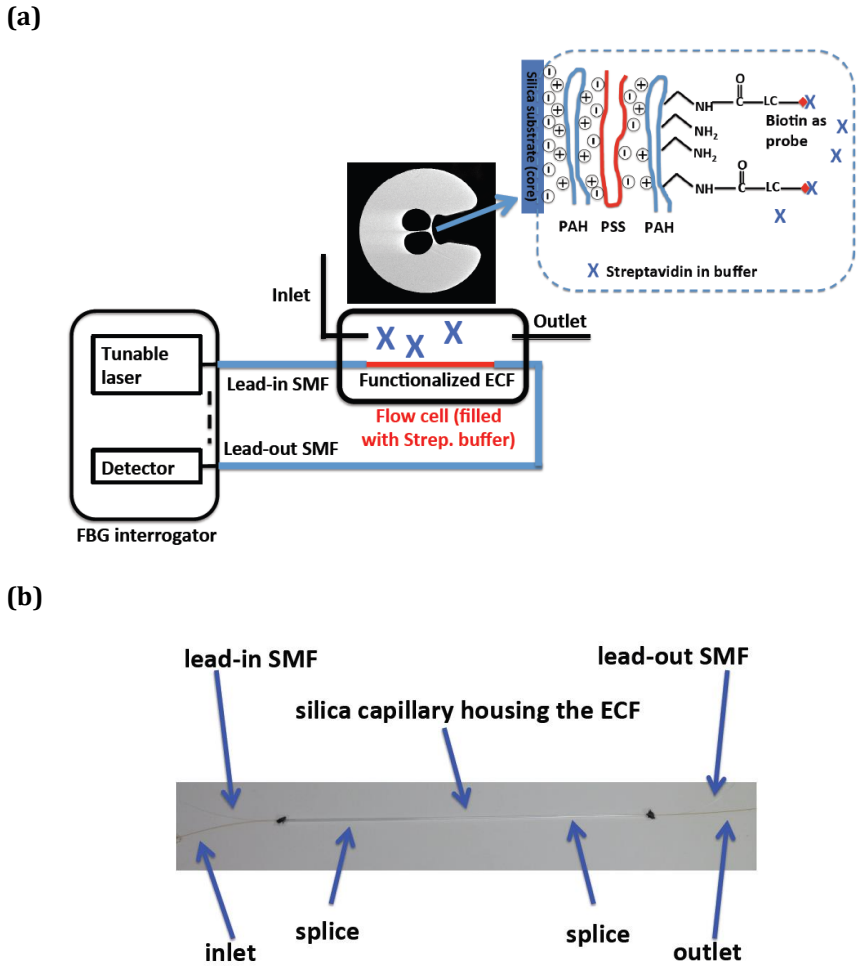

Fig. 2. (a) Schematic diagram of the final stage of the ECF core functionalized with biotin for detecting streptavidin suspended in buffer solution. The picture of the ECF cross section shown on the right side is a scanning electron microscope (SEM) image of the ECF used in this work. (b) An image of the sensor housed inside a silica capillary flow cell.

The proposed sensor was first tested with solutions with step-wise changes in RI, realized by dissolving different amounts of sodium chloride in deionized (DI) water, to verify its capability as an RI based sensing platform. The surface-functionalization using bio recognition molecules (biotin in this work) was carried out using the fuzzy nanoassembly technique [23]. First, positively charged poly(allylamine) hydrochloride (PAH, averaged molecular weight of 15 kDa, 2 mg/mL in 1M NaCl buffer, pH = 7, Sigma Aldrich) and negatively charged poly(sodium 4-styrene sulfonate) (PSS, averaged molecular weight of 70 kDa, 2 mg/mL in 1M NaCl buffer, Sigma Aldrich) were deposited alternately onto the fiber core surface using the layer by layer deposition technique described in [23], ending with a PAH layer (PAH/PSS/PAH) which provides amino groups for immobilization of biotin. In between depositing each layer, the sensor was rinsed extensively with 1M NaCl buffer. The deposition was performed by flowing corresponding solutions through the flow-cell using syringes and a pump system. NHS-Biotin (Ez-Link Sulfo-NHS-Biotin, Thermo Fisher) was freshly prepared at 0.5 mg/mL in phosphate buffer solution (PBS buffer, standard 1X, pH = 7.4, Sigma Aldrich) and flowed through for 1 hour, followed by extensive rinsing using PBS buffer to remove unbound biotin on the surface. After this step the sensor fabrication was considered complete. In the detection phase, streptavidin (Thermo Fisher) was freshly prepared at 0.2 mg/mL in PBS buffer and flowed though for 10 min at room temperature, then left inside the flow cell for 110 min followed by extensive rinsing with PBS. For the control experiment an ECF was prepared in the same way except that the attachment of

biotin was omitted. The duration of each functionalization step, including rinsing, was determined by observing the saturation of the phase change in real-time.

3. Results and Discussion

3.1. Transmission spectrum through the sensing device and the corresponding FFT

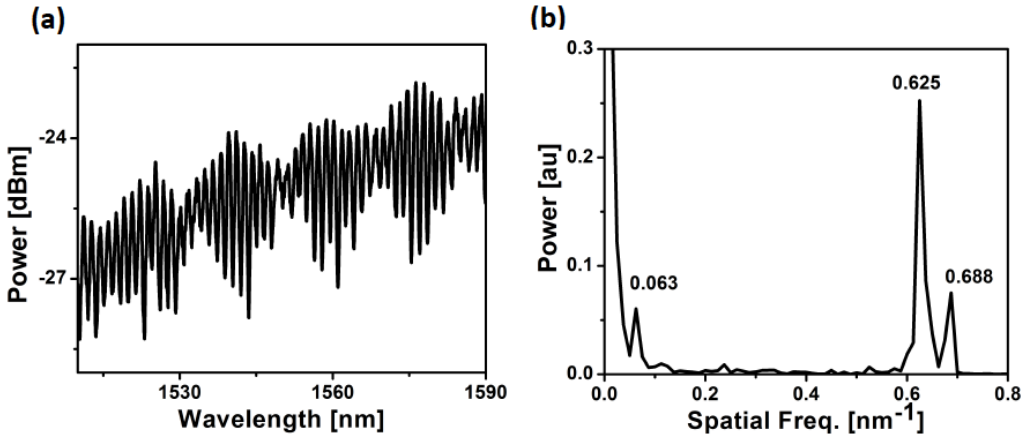

Fig. 3. (a) Transmission spectrum of the proposed sensing platform in DI water prior to functionalization and (b) its FFT showing three main peaks, indicating there were three dominantly excited modes in the ECF.

Fig. 3 shows the transmission spectrum (Fig. 3a) and its FFT (Fig. 3b) of the proposed device in DI water, without any attachment on the ECF core surface. As expected, there were more than two modes excited and propagated in the ECF section because the interference pattern in the wavelength domain is more complex than that of a simple sinusoidal waveform, typical of standard two-arm (mode) interference (Fig. 3a). FFT analysis of the transmission spectrum in Fig. 3a led to a spatial frequency spectrum with three main peaks at 0.063, 0.625 and 0.688 nm^{-1}, respectively. These three main spatial frequencies in Fig. 3b imply that there were three modes dominantly excited and interfered with each other forming the resultant interference pattern (Fig. 3a). Therefore, the complex spectrum in Fig. 3a can be considered as the superposition of three individual interference spectra formed by a specific pair of modes (pair of 1^{st}-2^{nd} modes, 1^{st}-3^{rd} modes and 2^{nd}-3^{rd} modes, respectively). Since the FSR is inversely proportional to the spatial frequency (smaller FSR → higher frequency), from Eq. 6 it can be seen that the effective index difference between two specific modes involved in an individual two-mode interference pattern will be linearly proportional to the spatial frequency. Larger effective index difference in turn means that the two modes involved in the interference pattern have very different evanescent power portions as they *"see"* the ECF core as well as the surrounding medium very differently. One therefore can expect that such a pair of modes will lead to a more sensitive response to change in the surrounding medium. On the other hand, modes of close effective indices should interact with the ambient medium quite similarly and thus an interference pattern formed by such modes will be less sensitive.

3.2. Refractive index sensing

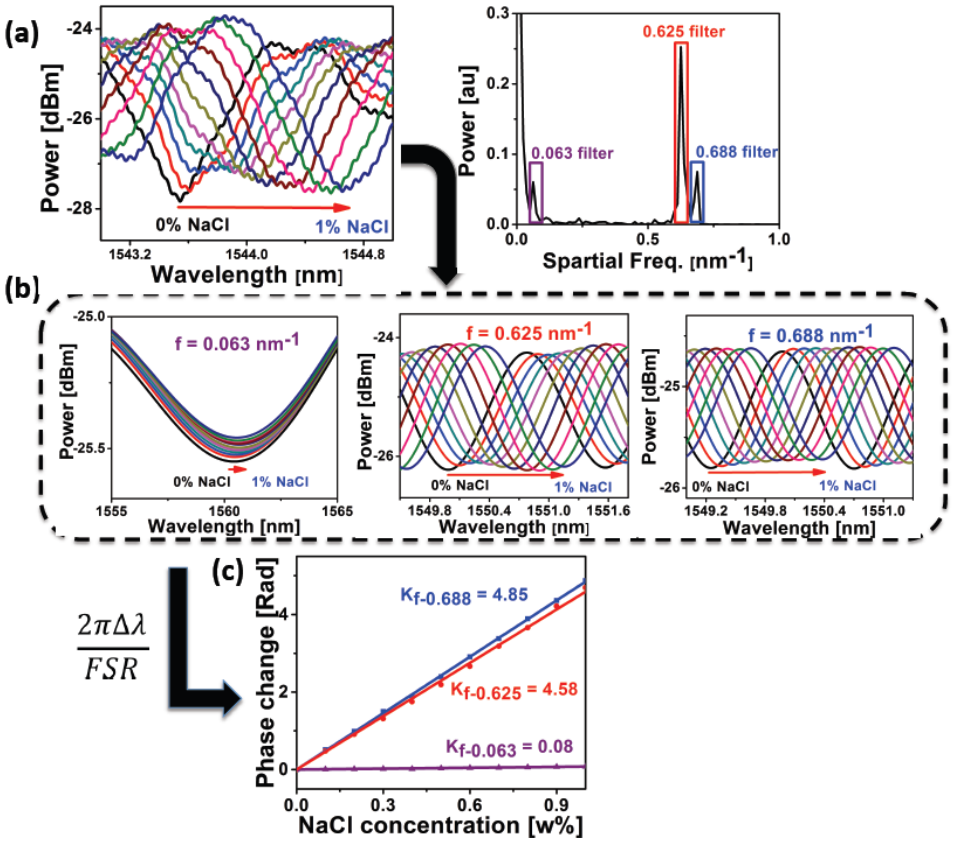

Fig. 4. (a) Raw spectrum of the proposed platform subjected to different ambient RI and (b) FFT-filtered spectra showing different amount of wavelength shifts for different spatial frequencies and (c) phase change at each spatial frequency computed from the wavelength shift values. f = spatial frequency of the FFT, K is the sensitivity (Rad/%) of the specified spatial frequency of the FFT.

Fig. 4a shows the zoomed transmission spectrum and its corresponding FFT of the sensor for stepwise increases in the surrounding refractive index by preparing sodium chloride solutions of different concentrations. As expected, the fringes shift to longer wavelengths, indicating that the phase has changed relatively between excited modes in the ECF. An analysis after FFT filtering reveals more detailed information, as can been seen in Figs. 4b and 4c. The fringes corresponding to the two large spatial frequencies (corresponding to two modes of large effective index difference) experienced a larger shift compared with that corresponding to the smaller spatial frequency. The sensitivity for the spectrum corresponding to the highest-intensity frequency of 0.625 nm^{-1} was estimated to be 667 nm/RUI. Fig. 4c shows the actual phase value computed at each spatial frequency by multiplying the wavelength shift with 2π and divided by the FSR or wavelength spacing between two adjacent interference minima at the fringe of interest. From Fig. 4c it can be seen that the proposed sensor can be used as a sensitivity-adjustable platform, as the FFT analysis is simply a software process that can be computed rapidly. In addition, in this type of sensor the phase sensitivity is directly proportional to the ECF length as shown in Eq. 4 and therefore should higher sensitivity be required, such as for sensing very small label-free molecules, a longer length of ECF can be used. Finally, higher order optical modes can also be utilized for the purpose of enhancing RI sensitivity of the platform, but it is not within the scope of this paper.

3.3. Biotin immobilization and streptavidin detection

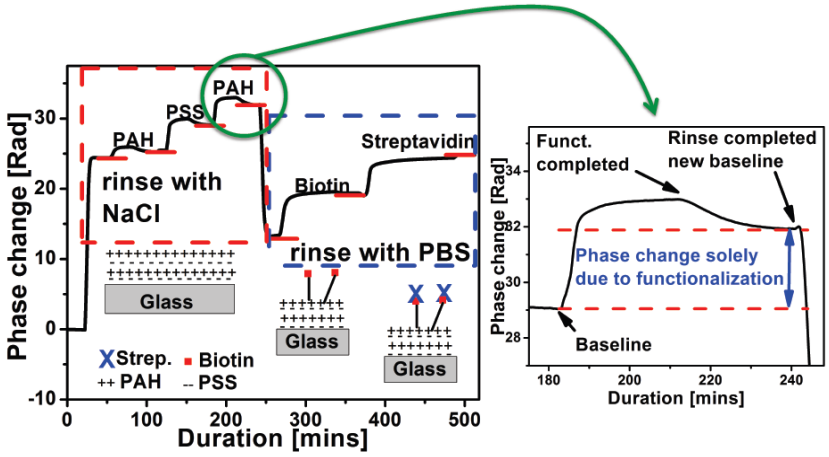

Fig. 5. Phase change of the sensing fiber at the spatial frequency of 0.625 nm^{-1} during the functionalization process (sensor fabrication completed after biotin immobilization) and streptavidin detection. The inset shows the zoomed phase change during the last PAH immobilization as an example of determining the final phase change due to molecular immobilization on the exposed fiber core surface.

The phase at the spatial frequency of 0.625 nm^{-1} was monitored during the entire process of passing different solutions through the flow cell to functionalize the surface of the sensor with biotin probes (Fig. 5). The spatial frequency of 0.625 nm^{-1} was used instead of the one with highest sensitivity at 0.688 nm^{-1} based on the fact that it corresponds to the interference between the two most strongly excited modes. Deposition of multiple layers of different molecules on the surface of the ECF not only changes the localized index, thus inducing phase changes on the propagating modes, but also increases the optical loss. Therefore it is preferable to use the most strongly excited modes for monitoring the phase change during the deposition of multiple layers. It should be noted that in principle one can always adjust the mode coupling condition between the lead-in SMF and the ECF to realize the spatial frequency with not only the highest sensitivity but also the highest sensitivity. The phase change responded as expected when subjected to different buffers (1M-NaCl and PBS buffer whose refractive indices are different). The surface attachment of a certain layer typically happens in three steps, shown as an example in the inset, for the case of attaching a positive layer of PAH to a negative layer of PSS. Starting from a baseline buffer, the phase at the chosen spatial frequency continuously increased as the buffer solution (the same baseline buffer but containing PAH) filled the flow cell, indicating immobilization activity of the PAH on the sensor's surface. The immobilization saturated when all of the binding sites on the surface have been covered. Rinsing of the functionalized surface with the buffer solution removed unbound molecules, creating a new baseline for the next immobilization step. The actual phase change due to the functionalization is obtained by comparing the baselines before and after the immobilization in the same buffer, ensuring that any spurious phase changes due to unbound molecules or slight differences in the background RIs (buffers solution containing different immobilization molecules) are removed (Fig 5 inset). This protocol is applied for every functionalization step, including functionalization with biotin as well as detection of streptavidin. The final changes after each functionalization step are represented by red bars in Fig. 5, where the phase signals were saturated after rinsing. The phase saturation was specified as when the phase fluctuation reached 0.01 rad, the phase noise level in our experiment. Using this value the RI detection limit in our experimental condition was estimated to be 3.8×10^{-6} RUI. For the case of immobilizing molecules such as biotin or streptavidin to the surface, the detection limit will depend largely on the particular immobilizing strategy as molecules immobilized at different distances from the surface will have different interaction with the evanescent field, and is beyond the scope of this paper.

It should be noted that in our experiment the time required to fill the flow-cell was approximately 10 min (0.1 ml/m) as faster rates were found to induce large phase fluctuations during filling. This could be attributed to the fact that the ECF was hung within the flow-cell by the two epoxy-anchors at the flow-cell ends and therefore could be sensitive to fast and abrupt changes in the flow. With a slow filling rate, the rise of the phase in the initial stage is however a combination of gradual bulk index change (as the new solution of different RI replaces the existing solution in the flow) and the localized index change at the ECF surface due to binding

and thus kinetic measurement of the binding activities, as in the case of chip-based SPR sensors [24, 25], is not yet possible in our proposed platform. Real-time kinetic measurement could be realized either by improvements in flow-cell design, e.g. create a trench along the flow-cell to accommodate the ECF to eliminate mechanical issues and allow for a faster filling rate, or by developing mathematical models of the binding kinetic taking into account the filling rate of the flow-cell, or both.

As shown in Fig. 5, after biotin was immobilized on the sensor surface as the capturing probe, the sensor was exposed to a buffer solution containing streptavidin as the target molecules. It can be seen that streptavidin binding to the biotin immobilized on the sensor surface leads to a significant increase in the phase, which was maintained after extensive rinsing of the sensor surface after streptavidin binding. The phase change due to streptavidin (molecular weight of 53kDa) being captured by biotin was approximately 5.5 rad, slightly smaller than the value of 6.02 rad for biotin (molecular weight of 0.25 kDa) being immobilized on the core surface. This could be attributed to a number of factors including: the much smaller concentration of streptavidin (≈0.029 mM) compared to that of biotin (≈1.13 mM) used in our experiment; the multivalent interaction between streptavidin and the immobilized biotin molecules as well as the actual physical dimension between the two (each streptavidin will bind to two biotins but physically blocking many immobilized non-binding biotins under it); and the possibility of steric hindrance contributing to a lower number of available probe binding sites for the target. It should also be noted that the streptavidin is located further away from the surface than biotin, thus limiting its interaction with the evanescent field of the propagating modes. To solve this problem one can reduce the number of polyelectrolyte layers (e.g. using just one PAH layer) at the expense of increase steric hindrance from the fiber surface as the probe is brought closer to the surface. Alternatively, the ECF core can be made smaller to enhance the evanescent field portion of the propagating modes [26], at the expense of increased fiber fabrication complexity and higher optical losses. Finally, one can use longer lengths of ECF to increase the interaction length, which is a simple route to enhance the sensitivity for applications in which sensing volume is not an issue. The optimized solution for this should likely be a combination of all the approaches mentioned, which is beyond the scope of this paper.

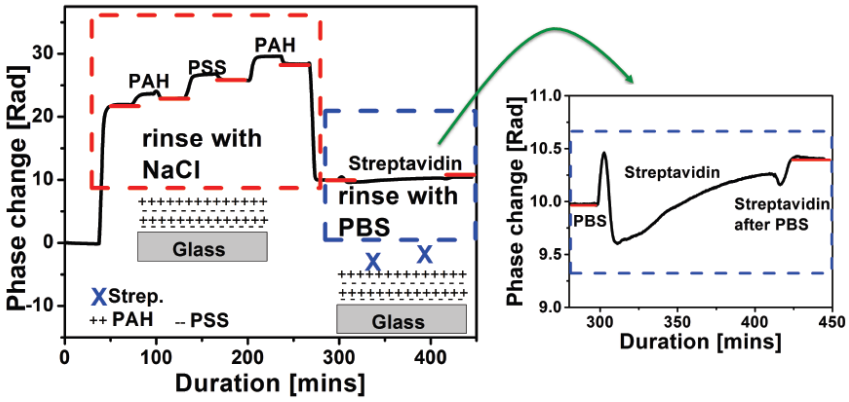

Fig. 6. Phase change of the control fiber subjected to the same functionalization process as in Fig. 5 except that the biotin immobilization (receptor probe) was omitted. Inset shows the zoomed phase change when streptavidin in BPS buffer was flown through the sensor surface, clearly indicated a very small phase change compared with the case of biotin-streptavidin binding.

In order to confirm that the binding in our case is indeed between biotin, the capturing probe, and streptavidin, the target molecule, a control sensor in which the biotin immobilization step was omitted was prepared (the length of control fiber was about 18.3 cm, leading to slightly smaller sensitivity compared with the sensing fiber) and subjected to the same streptavidin solution as shown in Fig. 6. The introduction of streptavidin did not result in a significant phase change (Fig. 6 inset) due to the absence of the biotin capture probe. The phase change in this case was only 0.4 rad, compared with 5.8 rad (about 15 times larger) for the case of biotin-streptavidin binding in Fig. 5. It should also be noted that in the case of the control experiment, any streptavidin molecules non-specifically captured to the surface due to adsorption will have

stronger interaction with the evanescent field (and thus induce a larger phase change) as it is closer to the surface than the case of biotin-streptavidin binding. Nevertheless, it is confirmed that the streptavidin phase change in Fig. 5 is due to the presence of the capturing probe biotin rather than spurious effects such as non-specific adsorption of streptavidin to the polyelectrolyte surface.

In an additional experiment (data not shown), we introduced a solution of bovine serum albumin (BSA, 1% Sigma Aldrich) onto the biotin-functionalized surface, which is a protein that does not specifically interact with the biotin probe. BSA is a protein with a molecular weight of 66.5 kDa, comparable to that of streptavidin (53 kDa), and is commonly used in biochemical assays to block the non-specific adsorption of proteins, such as antibodies, to the surface of microtitre wells or nitrocellulose membranes. Here BSA can also be considered as a model for non-target molecules that may be found in a tested sample. The exposure of the surface to BSA alters the baseline phase slightly (0.7 rad for overnight incubation) indicating some non-specific adsorption of BSA to the surface, or non-specific binding to biotin, or both. However, a subsequent exposure of the surface to the target molecule, streptavidin, still results in a larger phase change indicating probe availability for target capture. This comparatively larger phase change for streptavidin over BSA indicates the specificity of the biotin-streptavidin signal. It also demonstrates that a blocking step or alternative mechanisms (e.g. alternative functionalization, calibration fibers) may aid in reducing or accounting for the sensor's small amount of non-specific adsorption.

In conclusion, we have proposed what is, to the best of our knowledge, a novel sensing platform based on the multimode mode interference effect in an ECF. Our proposed platform can be used for label-free sensing of biological molecules as we have demonstrated detection of streptavidin using biotin as the capturing probe. There is, in principle, no restriction on using other biological capturing probes for a variety of target molecules. The proposed sensor structure is simple and can be mass-produced at relatively low cost as the platform fabrication is simply based on transverse alignment and fusion splicing between fibers, which can be readily automated. Its all-fiber configuration is highly stable compared with systems that use bulk-optic components and therefore could be useful for applications requiring in-field detection of biological compounds.

Acknowledgement
Linh Viet Nguyen and Kelly Hill acknowledge the support of the Australian Government's Cooperative Research Centres Program. Stephen Warren-Smith acknowledges the support of an Australian Research Council (ARC) Super Science Fellowship and is currently supported by the European Commission through the Seventh Framework Programme (FP7), PIIF-GA-2013-623248. Tanya Monro acknowledges the support of an ARC Georgina Sweet Laureate Fellowship and the ARC Centre of Excellence for Nanoscale Biophotonics. This work was performed in part at the OptoFab node of the Australian National Fabrication Facility (ANFF) utilizing Commonwealth and South Australian State Government funding. This work was supported via the Sensing Technologies for Advanced Reproductive Research (STARR) laboratory, supported by the South Australian State Government via the Premier's Science & Research Fund (PSRF) scheme. Authors thanks Alastair Dowler, Peter Henry, Anthony Leggatt, Roman Kostecki, and Heike Ebendorff-Heidepriem for their contribution to the silica fiber fabrication.

Reference
[1] J. Kirsch, C. Siltanen, Q. Zhou, A. Revzin, A. Simonian, Biosensor technology: recent advances in threat agent detection and medicine, Chem. Soc. Rev. 42 (2013) 8733-8768.
[2] S. M. Borisov, O. S. Wolfbeis, Optical biosensors, Chem. Rev. 108 (2008) 423-461.
[3] G. K. Knopf, A. S. Bassi ed., Smart Biosensor Technology, CRC Press, Taylor & Francis group, Boca Raton, 2008, pp. 589.
[4] A. P. F. Turner, , Chem. Soc. Rev. 42 (2013) 3184-3196.
[5] M. A. Arugula, A. Simonian, Novel trends in affinity biosensors: Current challenges and perspectives, Meas. Sci. Technol. 25 (2014) 032001.
[6] S. Song, H. Xu, C. Fan, Potential diagnostic applications of biosensors: current and future directions, Int. J. Nanomed. 1 (2006) 433-440.
[7] R. Singh, M. D. Mukherjee, G. Sumana, R. K. Gupta, S. Sood, B.D. Malhotra, Biosensors for pathogen detection: a smart approach towards clinical diagnosis, Sensor. Actuat. B-Chem. 197 (2014) 385-404.

[8] X. Fan, I. M. White, S. I. Shopova, H. Zhu, J. D. Suter, Y. Sun, Sensitive optical biosensors for unlabeled targets: a review, Anal. Chim. Acta 620 (2008) 8-26.
[9] K.-S. Mun, S. D. Alvarez, W.-Y. Choi, M. J. Sailor, A stable, label-free optical interferometric biosensor based on TiO2 nanotube arrays, ACS Nano 4 (2010) 2070-2076.
[10] A. Ymeti, J. S. Kanger, J. Greve, P. V. Lambeck, R. Wijn, R. G. Heideman, Realization of a multichannel integrated Young interferometer chemical sensor, Appl. Optics 42 (2003) 5649-5660.
[11] B. J. Luff, J. S. Wilkinson, J. Piehler, U. Hollenbach, J. Ingenhoff, N. Fabricius, Integrated optical Mach–Zehnder biosensor, J. Lightwave Technol. 16 (1998) 583-592.
[12] T. M. Monro, S. Warren-Smith, E. P. Schartner, A. François, S. Heng, H. Ebendorff-Heidepriem, S. Afshar V., Sensing with suspended core optical fibers, Opt. Fiber Technol. 16 (2010) 343-356.
[13] M. Dagenais, A. N. Chryssis, S. M. Lee, H. Yi, S. S. Saini, W. Bentley, Highly sensitive fiber Bragg grating biosensors, Proc. SPIE 5729 (2005) 214-224.
[14] A. Leung, P. M. Shankar, R. Mutharasan, A review of fiber-optic biosensors, Sensor Actuat. B-Chem. 8 (2007) 688-703.
[15] Z. He, F. Tian, Y. Zhu, N. Lavlinskaia, H. Du, Long-period gratings in photonic crystal fiber as an optofluidic label-free biosensor, Biosens. Bioelectron. 26 (2011) 4474-4478.
[16] L. V. Nguyen, S. C. Warren-Smith, A. Cooper, T. M. Monro, Molecular beacons immobilized within suspended core optical fiber for specific DNA detection, Opt. Express 20 (2012) 29378-29385.
[17] S. C. Warren-Smith, S. Afshar V., T. M. Monro, Theoretical study of liquid-immersed exposed-core microstructured optical fibers for sensing, Opt. Express 16 (2008) 9034-9045.
[18] S. C. Warren-Smith, H. Ebendorff-Heidepriem, T. C. Foo, R. Moore, C. Davis, T. M. Monro, Exposed-core microstructured optical fibers for real-time fluorescence sensing, Opt. Express 17 (2009) 18533-18542.
[19] R. Kostecki, H. Ebendorff-Heidepriem, C. Davis, G. McAdam, S. C. Warren-Smith, T. M. Monro, Silica exposed-core microstructured optical fibers, Opt. Mat. Express 2 (2012) 1538-1547.
[20] S. C. Warren-Smith, R. Kostecki, L. V. Nguyen, T. M. Monro, Fabrication, splicing, Bragg grating writing, and polyelectrolyte functionalization of exposed-core microstructured optical fibers, Opt. Express 22 (2014) 29493-29504.
[21] E. P. Diamandis, T. K. Christopoulos, The biotin-(strept)avidin system: principles and applications in biotechnology, Clin. Chem. 37 (1991) 625-36.
[22] S. C. Warren-Smith, S. Afshar V., T. M. Monro, Fluorescence-based sensing with optical nanowires: a generalized model and experimental validation, Opt. Express 18 (2010) 9474-9485.
[23] G. Decher, Fuzzy nanoassemblies: toward layered polymeric multicomposites, Science 277 (1997) 1232-1237.
[24] S. Lund-Katz, D. Nguyen, P. Dhanasekaran, M. Kono, M. Nickel, H. Saito, M. C. Phillips, Surface plasmon resonance analysis of the mechanism of binding of apoA-I to high density lipoprotein particles, J. Lipid Res. 51 (2010) 606-617.
[25] P. Schuck, H. Zhao, The role of mass transport limitation and surface heterogeneity in the biophysical characterization of macromolecular binding processes by SPR biosensing, in: N. J. de Mol, M. J. E. Fischer (eds.), Surface Plasmon Resonance, Methods in Molecular Biology **627**. Springer Science+Business Media, Berlin (2010) 15-54.
[26] Y. Zhu, H. Du, and R. Bise, Design of solid-core microstructured optical fiber with steering-wheel air cladding for optimal evanescent-field sensing, Opt. Express 14 (2006) 3541-3546.